Trace Amounts of Multifunctional Electrolyte Additives Enhance Cyclic Stability of High-rate Aqueous Zinc-Ion Batteries

Haoyu Feng[a], Weihua Zhou[a], Zhuo Chen[a], Ziming Wan[a], Jian Wang[a], Lin Sheng[b], Lun Zhang[c], Shuaipeng Hao[d], Hongzhen He[e], Hao Gu[c], Feng Ryan Wang[c], Zhangxiang Hao[a], Junrun Feng*[a]

- [a] School of Science, School of Chip Industry, Hubei University of Technology, Wuhan, Hubei 430068, China
- [b] School of Mechanical and Electronic Engineering, Suzhou University, Suzhou, Anhui 234000, China
- [c] Materials and Catalysis Laboratory, Department of Chemical Engineering, University College London, London WC1E 7JE, United Kingdom
- [d] State Key Laboratory of Material Processing and Die & Mould Technology, School of Materials Science and Engineering, Huazhong University of Science and Technology, Wuhan, Hubei, 430074, China.
- [e] Department of Earth Science and Engineering, Imperial College London, London, SW7 2AZ, UK *Corresponding author. E-mail: fengjunrun@hbut.edu.cn

Abstract: Aqueous zinc ion batteries (AZIBs) are renowned for their exceptional safety and ecofriendliness. However, they face cycling stability and reversibility challenges, particularly under high-rate conditions due to corrosion and harmful side reactions. This work introduces fumaric acid (FA) as a trace amount, suitable high-rate, multifunctional, low-cost, and environmentally friendly electrolyte additive to address these issues. FA additives serve as prioritised anchors to form water-poor Inner Helmholtz Plane on Zn anodes and adsorb chemically on Zn anode surfaces to establish a unique *in-situ* Solid-electrolyte interface. The combined mechanisms effectively inhibit dendrite growth and suppress interfacial side reactions, resulting in excellent stability of Zn anodes. Consequently, with just tiny quantities of FA, Zn anodes achieve a high Coulombic efficiency of 99.55% and exhibit a remarkable lifespan over 2580 hours at 5 mA cm⁻², 1 mAh cm⁻² in Zn//Zn cells. Even under high-rate conditions (10 mA cm⁻², 1 mAh cm⁻²), it can still run almost for 2020 hours. Additionally, the Zn//V₂O₅ full cell with FA retains a high specific capacity of 106.95 mAh g⁻¹ after 2000 cycles at 5 A g⁻¹. This work provides a novel additive for the design of electrolytes for high-rate AZIBs.

Keywords: aqueous zinc-ion batteries, electrolyte additives, high-rate, solid-electrolyte interfaces, electric double layers

1. Introduction

Given the pressing requirement for carbon neutrality, there is a growing demand for renewable energy sources and the corresponding need for large-scale energy storage systems. [1-3] Among these, Lithiumion batteries are widely recognized for their high energy density, broad applicability, and environmental friendliness. [4,5] Despite their market dominance and technological advancements, lithium-ion batteries face low safety, scarce resources, and high costs, which hinder their suitability for expansive energy storage applications. [6,7] Aqueous zinc ion batteries (AZIBs) provide higher safety with aqueous electrolytes and exhibit advantages like low redox potential (-0.7626 V vs. SHE), high theoretical specific capacity (820 mAh g⁻¹), and so on, making them a prominent area of research for large-scale energy storage. [8–10] However, AZIBs encounter challenges with Zn anodes and electrolytes, including the hydrogen evolution reaction (HER), corrosion, side reactions, and zinc dendrite growth. [11,12] Water molecules corrode the zinc electrode, generating by-products like Zn₄SO₄(OH)₆·xH₂O(ZHS), resulting in an uneven electric field, inhomogeneous ion distribution, and uncontrolled zinc ion migration, which can lead to crazy dendrite growth and potential short circuits. [13,14] Additionally, corrosion depletes electrolytes, and HER could pose safety concerns. [15,16]

To navigate these tricky hurdles, various strategies encompassing surface optimization, interfacial engineering, and electrolyte modification have been proposed to fortify interfacial compatibility between zinc electrodes and aqueous solutions, curb side reactions, and extend battery life. For instance, Dong et al. used a PES/SPEEK-based CEM coating with zinc-friendly hydrophobicity to achieve fast zinc deposition kinetics and long-term cycle life, while Ai et al. designed a 2D-mPDA mimetic superstructure as a protective layer for zinc. Among these, electrolyte modification emerges as a straightforward and productive method to bolster AZIBs performance by enhancing the compatibility between the Zn anodes and the aqueous electrolyte interface. Achieving long-term stable Zn anodes under high-rate conditions remains challenging for practical rechargeable zinc ion batteries. Although there have been many kinds of literature (e.g., the introduction of zinc gluconate (ZG) by Xu et al., ethylenediaminetetracetic acid disodium salt (EDTA-2Na) by Xu et al. and phytic acid (PA) by Wang et al.), have demonstrated that electrolyte additives can significantly improve battery performance by altering the Zn²⁺ solvation structure. However, strong coupling between Zn²⁺ and additives often results in inferior reaction kinetics, particularly under high-rate conditions, reducing battery cycling stability. Considering that the electrochemical reactions occur in the electric double layer (EDL),

controlling the EDL at the anode/electrolyte interface is crucial for assessing and enhancing electrode stability and electrochemical performance. [24–26] To develop high-rate AZIBs, exploring novel additives capable of modulating the EDL structure is crucial in desolvation and zinc ion reduction. Additionally, these additives should exhibit weak coupling with Zn²⁺ to ensure sufficient Zn²⁺ mobility under high-rate conditions. [27,28] Specific group-containing additives can homogeneously adsorb on Zn anode surfaces, regulating the EDL and preventing direct contact between reactive water molecules and Zn anodes, inducing homogeneous Zn²⁺ deposition.^[27] For example, Chen et al. chose citrulline (Cit), and Hu et al. introduced cerium chloride (CeCl₃) as an electrolyte additive to regulate the EDL.^{[7][28]} Although these additives enhance the stability of Zn anodes to a certain extent, they have drawbacks such as requiring high amounts, being costly, and lacking environmental friendliness. Considering practical industrial production requirements, developing a novel electrolyte additive that is trace, suitable for high-rate performance, low-cost, and environmentally friendly has become a challenging and significant task. Inspired by the strong adsorption properties of molecules with carboxylic acid groups on Zn anodes surfaces, we propose using fumaric acid (FA), a highly polar group (-COOH) containing, trace, suitable for high rate additive to efficiently modulate the EDL structure on Zn anodes and construct an in-situ stabilized solid-electrolyte interface (SEI). [15][29] Theoretical analysis and experimental tests indicated that FA operates via two synergistic mechanisms:(I) FA's carboxylic acid groups undergo competitive adsorption on Zn anodes, forming a water-poor Inner Helmholtz Plane (IHP), inhibiting hydrogen evolution corrosion of free water molecules on Zn anodes. (II) FA adsorption facilitates the formation of a stable zinc-friendly SEI, inhibits corrosion, regulates Zn²⁺ plating/stripping behaviors, and promotes uniform Zn deposition. These mechanisms significantly suppress corrosion, harmful side reactions, and dendrite proliferation, improving the Zn anode's stability and reversibility. Consequently, with just tiny quantities of FA, the Zn//Zn cells exhibit extra-long cycling stability of over 3410 hours at 5 mA cm⁻²,1 mAh cm⁻², and up to 1800 hours under 10 mA cm⁻², 1 mAh cm⁻² high-rate conditions, contrasting sharply with cells using ZnSO₄. Meanwhile, the zinc electrode in FA-modified electrolyte shows excellent plating/stripping reversibility, with an average Coulombic efficiency of 99.55%. Additionally, the Zn//V₂O₅ full cell with FA retains a high specific capacity of 106.95 mAh g⁻¹ after 2000 cycles at 5 A g⁻¹

2. Results and discussion

To investigate the effects of varying the FA additives concentrations on zinc battery performance, we

designed a concentration gradient experiment using 2 m ZnSO₄ electrolyte with varying FA concentrations: 2 m ZnSO₄ (FA 0), 2 m ZnSO₄ + 2 mmol FA (FA 2), 2 m ZnSO₄ + 4 mmol FA (FA 4), and 2 m ZnSO₄ + 8 mmol FA (FA 8). The contact angles of the ZnSO₄ electrolyte with FA additives were lower than the FA 0 electrolyte, with the FA 4 electrolyte exhibiting the smallest contact angle (**Figure** 1a). This suggests enhanced wettability at the electrolyte-Zn foil interface, likely due to the adsorption of FA, which contains carboxylic acid groups known for their strong affinity towards Zn. [15][30] Meanwhile, through Density functional theory (DFT) calculations, we analyzed the adsorption energies of FA molecules on the zinc surface, comparing vertical (ZF-V) and parallel (ZF-P) orientations. Results showed a stronger preference for parallel adsorption, with significantly lower energy values (-0.653 eV for ZF-V and -0.817 eV for ZF-P) compared to the adsorption energy of H₂O molecules alone, indicating a more stable FA attachment in a parallel configuration on the zinc surface (**Figure 1b**).^[31] The electrochemical interface formed by the contact between the solid electrode and the liquid electrolyte is referred to as the double electric layer (EDL), which consists of a dense layer (CL) and a diffuse layer (DL). The CL located inside the bilayer is further divided into the inner Helmholtz plane (IHP) and the outer Helmholtz plane (OHP), where the inner dense layer closest to the electrode is referred to as the IHP. The structure of the IHP greatly influences the performance of the cells due to the adsorption, detachment, and migration of the zinc ions, and the key steps in the electrochemical processes such as electron transfer that occur at the IHP.[32] Cyclic voltammetry (CV) tests further validated the impact of FA, showing an obvious decrease in double electric layer capacitance values (208.46 µF cm⁻² for FA 0 vs. 135.67 μF cm⁻² for FA 4) (**Figure 1c, S1**). This reduction may be attributed to the adsorption of fumaric acid, which has a larger molecular size than water molecules, onto the IHP, resulting in an increase in the thickness of the double electric layer. Upon addition of FA, FA molecules competed with H₂O molecules for preferential adsorption onto the IHP, turning the IHP, which was originally filled with H₂O molecules, into a water-poor IHP formed by FA adsorption (Figure 1d). [5][33] To further demonstrate the change of IHP structure in electrolytes with FA, based on the capacitive adsorption in the non-faradaic double electric layer, we verified that FA competes with H2O for preferential adsorption on IHP by AC voltammetry. The test results showed that the capacitance tested in FA 4 electrolyte was lower than that tested in FA 0 electrolyte and the potential of zero charge (PZC) decreased from 0.83 V to 0.79 V, suggesting that the FA preferentially adsorbed in the IHP and altered the IHP structure (Figure S20). [34– ^{37]} Furthermore, Fourier-transform infrared (FTIR) and Raman spectra indicated an extremely weak

coupling of FA to Zn²⁺ (Figure S2,3). In the FTIR spectra, the additive FA does not cause relatively significant peak shifts, suggesting that FA has little effect on the solvated structure. Meanwhile, Raman spectroscopy tests verified this. The Raman spectral spectra of the electrolyte with or without FA almost overlapped, indicating that the molecular vibrational modes and ion-solvent interactions in the two electrolytes are almost the same, the coupling between FA and zinc ions is very weak. Nuclear magnetic resonance (NMR) tests showed that the addition of FA to ZnSO₄ resulted in a positive chemical shift of the ¹H peak of D₂O, suggesting that the interaction between FA and H₂O molecules could reshape the hydrogen-bonded structure of the H₂O molecules in the FA 4 electrolyte, thus reducing the contact between the active H₂O molecules and the Zn anodes (Figure S4).^[38] Additionally, linear scanning voltammetry (LSV) tests showed that the HER starting potential of the electrolyte with FA was negatively shifted, indicating that FA additives inhibit HER by preferentially adsorbing to prevent reactive water molecules from directly contacting Zn anodes (Figure 1e). [16] As shown in Figure S19, when the concentration of FA was increased to 20 mmol there were fumaric acid particles that were not completely dissolved. Meanwhile, LSV testing of each of the other concentration gradients showed that the strongest inhibition of HER was found at a concentration of 4 mmol of the additive FA (Figure S18). Chronoamperometry (CA) curves revealed a consistent increase in the Zn anodic current over 350 s in the FA 0 electrolyte, attributed to a two-dimensional diffusion process of Zn²⁺, potentially leading to significant dendrite formation (Figure 1f). When zinc ions reach the electrode surface in a 2D diffusion mode, localized areas may have too high a concentration of zinc ions, leading to uneven deposition. [39] In contrast, in the 3D diffusion mode, the zinc ions can diffuse freely throughout the space without being restricted to a specific direction, resulting in a more uniform zinc ion concentration on the electrode surface. Thus, the 3D diffusion mode helps to achieve uniform zinc deposition on the electrode surface. [40] In stark contrast, Zn plating in the electrolytes with FA showed a nearly unchanged current density. This suggests that FA's preferential adsorption minimizes energy barriers for Zn²⁺ lateral diffusion, optimizes electric field distribution, and regulates Zn ion flux, promoting stable three-dimensional diffusion. [41,42] Lastly, charge transfer resistance (Rct) measurements indicated that symmetric cells containing FA generally exhibited lower R_{ct} values than those without FA, pointing to a faster charge transfer process and enhanced zinc ion mobility in the modified cells, offering the potential for the development of highrate capable AZIBs (**Figure 1g, S5**).^[30,43]

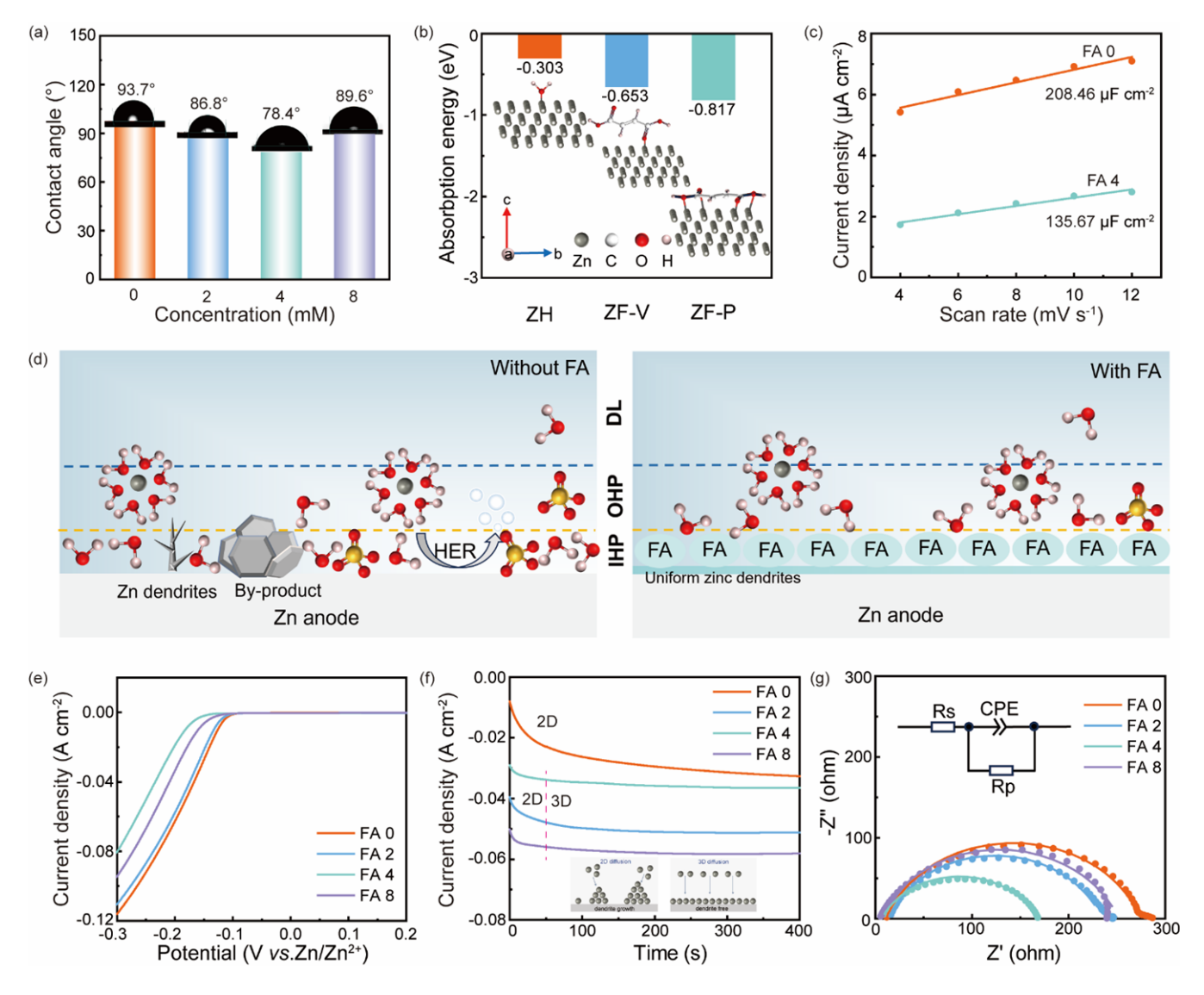


Figure 1. a) Contact angle test plots of Zn surfaces with FA 0, FA 2, FA4, and FA 8 electrolytes, respectively. b) Adsorption models and corresponding adsorption energies of H₂O and FA molecules on the Zn (002) plane. c) The EDL capacitance for cells with FA 0 and FA 4 electrolytes. d) Schematic diagram of Zn deposition behavior in FA 0 and FA 4 electrolytes. e) LSV curves of Zn//Zn symmetric cells tested in various electrolytes. f) CA curves of the symmetric cells with various electrolytes. g) EIS impedance of symmetric cells with various electrolytes.

Without FA, direct exposure of the electrolyte to unstable Zn anodes leads to corrosion and uncontrollable HER parasitic reactions, resulting in the creation of detrimental by-products like Zn₄SO₄(OH)₆·xH₂O (ZHS), as depicted in **Figure 2a**.^[44] Conversely, incorporating FA into electrolytes enables FA-Zn adsorption on the Zn surface. This interaction with Zn anodes results in the forming of an *in-situ* solid-electrolyte interface (SEI) layer. This layer facilitates homogeneous nucleation sites, effectively inhibiting the HER (**Figure 2a**). To further investigate the mechanism of FA-induced *in-situ* SEI layer formation,

bare Zn foils were soaked in two types of electrolytes (FA 0 and FA 4) for 48 h. Observations highlighted in Figure 2b, c reveal that the Zn foil surface in the FA 0 electrolyte was uneven, in stark contrast to the smooth surface of the Zn flakes submerged in the FA 4 electrolyte. Furthermore, disorganized and fragmented corrosion by-products appeared on the Zn foil exposed to the FA 0 electrolyte for 48 h (Figure S6). In contrast, the Zn foil's surface in the FA 4 electrolyte developed a translucent white coating. [45] With the aid of a high-resolution field emission scanning electron microscope, we can clearly observe that a layer of *in-situ* SEI with a thickness of about 2 µm was formed on the surface of the zinc foil soaked in the FA 4 electrolyte for 48 h, which is demarcated from the surface of the zinc foil (Figure 2c). Additional analysis via X-ray diffraction (XRD) showcased in Figure 2d, including Zn foils immersed in FA 0 and FA 4 electrolytes for 48 h and bare Zn foil, presented diffraction peaks at 36.292°, 38.992°, and 43.231° respectively (PDF#04-0831), with a novel diffraction peak at 7.309° corresponding to FA 0 soaked foil, linked to the by-product Zn₄SO₄(OH)₆·5H₂O. This signifies FA's potent efficacy in curbing Zn anode corrosion. In further scrutinizing the in-situ SEI layer formation, a comparison of Fourier transform infrared spectra (FTIR) of bare Zn, FA, and Zn foil immersed for 48 hours in FA 4 electrolyte showing a peak shift related to the carboxyl group (COOH) at 1640 cm⁻¹(Figure 2e). [46] Moreover, X-ray photoelectron spectroscopy (XPS) evidenced a slight uptick in the binding energy of Zn 2p 3/2 and Zn 2p 1/2 for the Zn foil soaked in the FA 4 electrolyte versus the FA 0 electrolyte, attributed to the interplay of FA's COOH groups with the Zn foil leading to the formation of Zn-O bonds, alongside C=O (533 eV) and Zn-O (530.2 eV) detected in the O 1s spectrum (Figure 2f, g). These results consistently confirm that adding FA induces the formation of an *in-situ* SEI layer. [47] Further to explore the composition of SEI, we first performed elemental analysis tests on the surface of SEI with energy dispersive spectroscopy (EDS), and as the results are shown in Figure S23, a large amount of C and O elements appeared on the surface of the zinc foil, which initially indicated that FA might have reacted with the zinc foil to generate some kind of compound film layer. This was also confirmed by the elemental analysis of the SEI cross-section (Figure S21). Then Raman spectroscopy tests were performed to analyze the changes on the surface of the zinc foil before and after immersion (Figure S22), and the characteristic peaks at about 1000 cm⁻¹, 1550 cm⁻¹, and 1650 cm⁻¹ of the immersed zinc foil were related to the C=O asymmetry, symmetric tensile vibration, and C-H vibration, respectively, which further confirmed that fumaric acid reacted with zinc by complexation, and may form *in-situ* SEI layers composed mainly of zinc fumarate. [48] Since the surface structure of the formed *in-situ* SEI layer is loose, this non-dense structure allows zinc ions to pass through

the SEI layer during the battery cycling process (Figure S23). According to the elemental analysis diagram of the cycled Zn anodes cross-section, it can be seen that there is relatively less zinc distribution at the interface between the SEI and the zinc foil, and more zinc distribution in the region close to the SEI layer, so it can be speculated that zinc ions were mainly deposited in the interior below the SEI during the cycling process (Figure S27). To investigate the protective effect of FA additives on Zn electrodes, we tested the Tafel curves of various electrolytes (Figure 2h). Compared with FA 0 electrolytes, the corrosion potentials of FA 2, FA 4, and FA 8 electrolytes are positively shifted. The corrosion current densities of FA 0, FA 2, FA 4, and FA 8 electrolytes are 0.941 mA cm⁻², 0.887 mA cm⁻², 0.690 mA cm⁻² ², and 0.712 mA cm⁻², respectively, suggesting that the FA-induced SEI layer acts as a bulwark against Zn anode corrosion. [49] Comparison of cyclic voltammetry (CV) curves of Zn//Ti asymmetric cells with various electrolytes, depicted in Figure 2i, and voltage curves of Zn//Zn symmetric cells tested at 2 mA cm⁻² (Figure 2j) further validate that the electrolytes with FA enhances redox current density and decreases nucleation overpotentials(46.8 mV for FA 0, 42.7 mV for FA 2, 35.4 mV for FA 4, and 39.2 mV for FA 8), which indicates that the *in-situ* SEI layer can promote zinc ion transport and augment reaction kinetics. Compared with FA 0 (84.2 mV), FA 2, FA 4, and FA 8 nucleation overpotentials are 68.6 mV, 47.5 mV, and 73.6 mV, respectively. This notable decrease in nucleation overpotentials, indicative of a reduced barrier to Zn plating, supports uniform nucleation and Zn growth, attributed to the in-situ SEI layer's role in offering consistent nucleation sites and harmonizing the electrode surface's electric field, hence lowering the nucleation overpotential. [20]

To further prove the modulatory effects of FA additives on the zinc electroplating process, we designed *in-situ* optical visualization experiments to capture the real-time dynamics of Zn²⁺ deposition across different electrolytic environments. **Figure 3a, b** highlights that in the FA 0 electrolyte, the initial deposition phase on the Zn foil is characterized by sharp protrusions, rapidly evolving into extensive Zn dendrite proliferation as the deposition progresses. In stark contrast, the introduction of FA markedly alters this landscape, where crazy-growing zinc dendrites are notably absent, and the deposition layer maintains a very flat profile, tentatively confirming FA's capability to modulate Zn²⁺ deposition towards achieving a uniform and dendrite-free coating. ^[50] This modulatory effect of FA is further corroborated by scanning electron microscopy (SEM) imaging, displaying both surface and cross-sectional views of the Zn anodes. The Zn anodes with FA 0 electrolyte are besieged by vertical, erratic by-product formations and chaotic zinc dendrite structures, indicative of heterogeneous Zn²⁺ deposition (**Figure 3c, d, S6-9**).

Conversely, Zn anodes subjected to the FA 4 electrolyte reveal a morphological transformation to a flat, hexagonal, close-packed layout, presenting a substantially smoother appearance than the FA 0 electrolyte. Atomic force microscopy (AFM) demonstrated the surface roughness associated with zinc deposition under both conditions, further confirming these observations (**Figure 3e, f**). [44] This improvement is attributed to the presence of a homogeneous solid-electrolyte interface (SEI) layer consisting of FA-Zn complexes, which not only plays a vital role in inhibiting the parasitic reaction but also in regulating the pathway of Zn²⁺ electroplating/stripping, effectively thwarting the emergence of Zn dendrites. X-ray diffraction (XRD) testing of the circulated Zn anodes showed a significant reduction in the intensity of the characteristic ZHS with the FA 4 electrolyte compared to the FA 0 electrolyte, suggesting effective mitigation of the harmful parasitic side reactions (**Figure S10**). Additionally, the ratio of the peak Zn (002) plane to the peak Zn (100) plane of the cycled Zn anodes was significantly increased (2.60 for FA 4 and 1.25 for FA 0), suggesting that FA additives modulate Zn²⁺ flux and facilitate homogenous Zn²⁺ deposition along the Zn (002) plane, ultimately realizing dendrite-free Zn anodes.

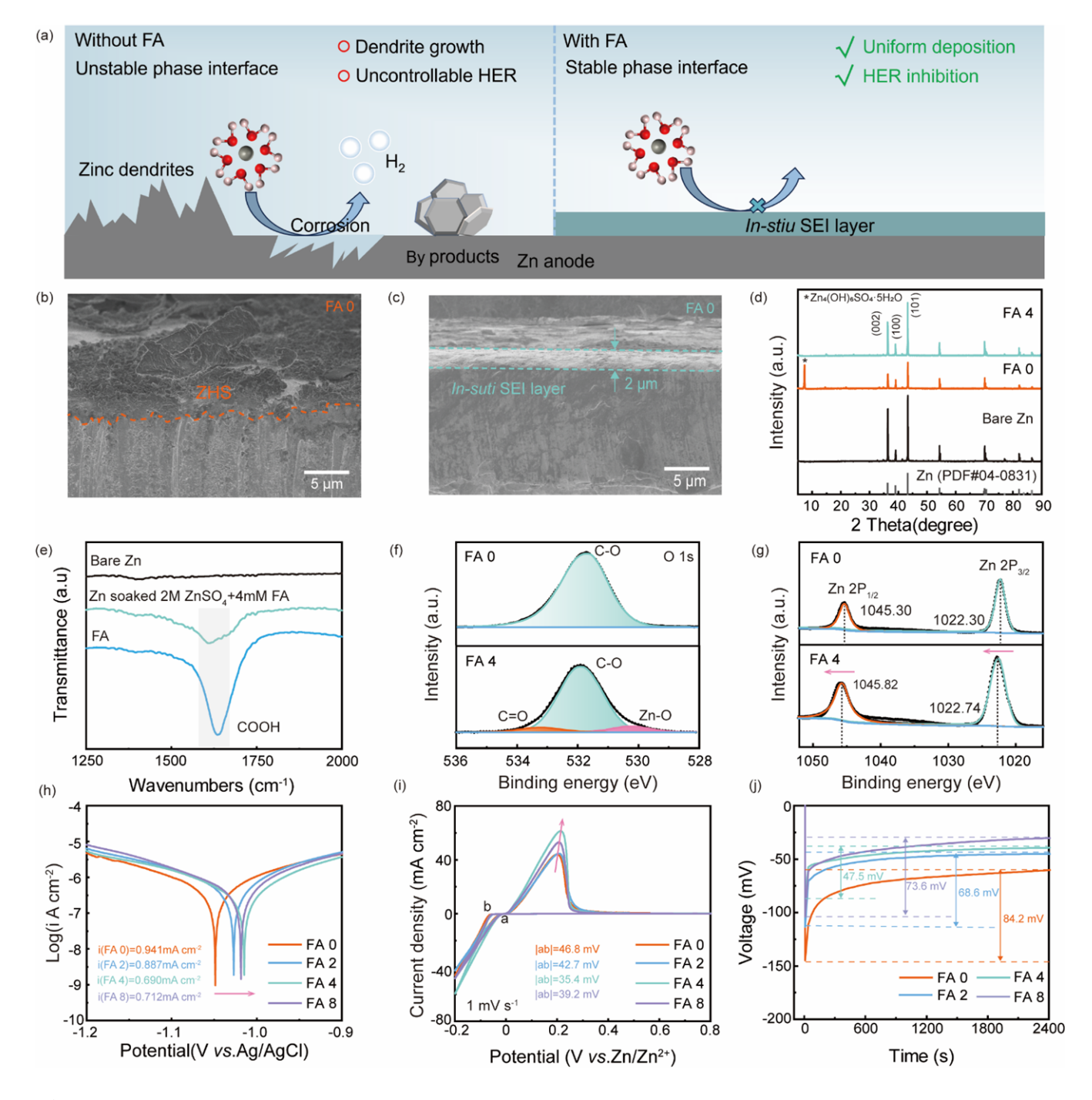


Figure 2. a) Schematic of the zinc deposition mechanism in electrolytes with or without FA. b) Cross-sectional SEM images of the zinc foil soaked in FA 0 electrolyte for 48 h. c) Cross-sectional SEM images of the zinc foil soaked in FA 4 electrolyte for 48 h. d) XRD patterns of bare Zn, Zn foil soaked in FA 0 electrolyte for 48 h, and Zn foil soaked in FA 4 electrolyte for 48 h. e) Comparative FTIR plots of bare Zn, FA, and Zn foil soaked in FA 4 electrolyte for 48 h. The XPS comparison chart of f) O 1s and g) Zn 2p on the surface of Zn foil soaked in the FA 0 and FA 4 electrolytes. h) Tafel curves of Zn foils in various electrolytes. i) Comparison of CV curves of Zn//Ti cells with various electrolytes. j) Voltage profiles and nucleation overpotentials of Zn//Zn cells with various electrolytes at a current density of 2 mA cm⁻².

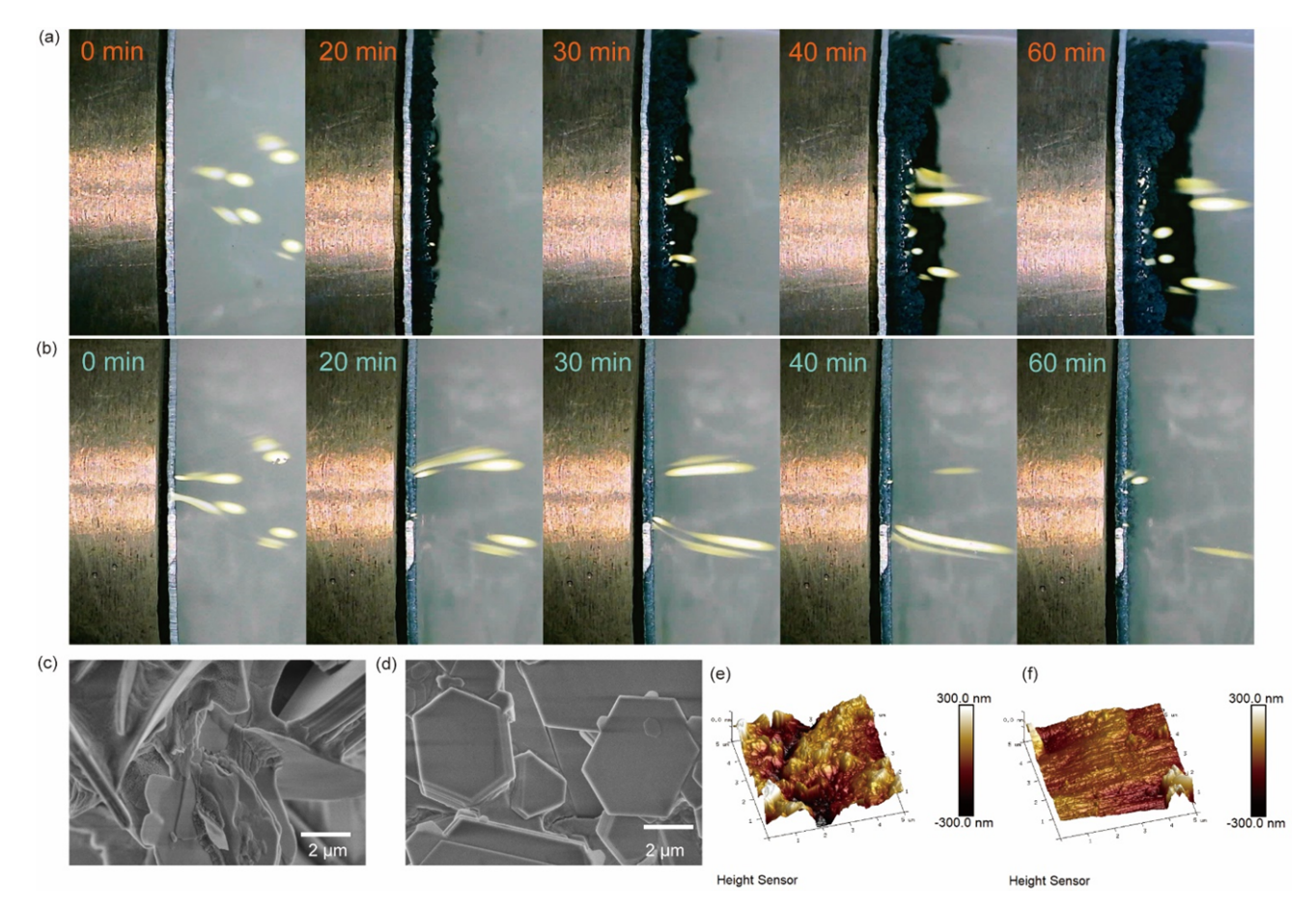


Figure 3. *In-situ* optical microscopy process images of the cross-sectional Zn deposition morphology on Zn electrode at 15 mA cm⁻² with a) FA 0 and b) FA 4 electrolytes. The SEM images of the Zn anode surface cycled for 200 cycles at 5 mA cm⁻²,1 mAh cm⁻² with c) FA 0 and d) FA 4 electrolytes. AFM images of the Zn anodes surface cycled for 200 cycles at 5 mA cm⁻²,1 mAh cm⁻² with e) FA 0 and f) FA 4 electrolytes.

To evaluate the cycling stability of FA additives, we subjected Zn//Zn symmetric cells with various electrolytes to long-cycle tests. Under 5 mA cm⁻² and 1 mAh cm⁻² conditions, the cell employing FA 0 electrolyte succumbed to a short circuit at 110 hours. In stark contrast, incorporating FA into the electrolytes of Zn//Zn symmetric cells led to a dramatic surge in cycling efficacy. Notably, the cell integrating FA 4 electrolyte showcased impressive cycle durability, operating stably for an extended period of 2580 hours without any noticeable irreversible voltage (**Figure 4a**). Moreover, the cycling stability in the FA 4 electrolyte is dramatically improved at higher current densities and higher areal capacities. (2020 hours *vs.* 33 hours at 10 mA cm⁻²,1 mAh cm⁻² *vs.* 1730 hours vs. 107 hours at 5 mA cm⁻²,2 mAh cm⁻²), as detailed in **Figure 4b, c**. Studying the cycle life of batteries with higher depth of discharge (DOD) allows for a more accurate estimate of their usable energy density and lifetime. [51] To more accurately assess its usable energy density and lifespan, we conducted performance tests at higher

depths of discharge (DOD) using a 50 µm zinc foil. [8] Under test conditions of 1 mA cm⁻² and 5 mAh cm⁻ ² (DOD of 19.3%) (Figure S24), it is evident that FA 4 exhibits greater stability compared to FA 0, achieving a cycle time of 180 hours. Additionally, at 10 mA cm⁻² and 5 mAh cm⁻² (DOD of 19.3%) (Figure S25), the cycle time reached 200 hours. Cycling over 190 hours at 1 mA cm⁻², 10 mAh cm⁻² (DOD of 38.6%) (Figure S26), further demonstrates the potential of FA additives for practical applications.^[52] To compare the rate performance of Zn//Zn symmetric cells with various electrolytes, with a fixed areal capacity of 1 mAh cm⁻², the current density was varied to 1, 2, 5, 10, 20, and 1 mA cm⁻² ² (**Figure 4d**). Remarkably, while the symmetric cell incorporating FA 0 electrolyte and its counterpart with the FA additive demonstrated comparable polarization voltages at lower current densities, a significant reduction in polarization voltage was observed at higher current intensities for the cell with the FA-modified solution, evidencing accelerated Zn²⁺ migration which illustrates the additive's effectiveness in high-rate applications.^[53] Additionally, to delve into the impact of FA additives on the reversibility of Zn deposition/stripping processes, asymmetric Zn//Cu cells with various electrolytes were crafted and evaluated under a current density of 2 mA cm⁻² and an aerial capacity of 1 mAh cm⁻². As delineated in Figure S11-13, the Zn//Cu cell with FA 4 electrolyte demonstrated a tenfold increase in cycling stability relative to the cell with FA 0 electrolyte, marking a significant performance enhancement and achieving an extraordinary average Coulombic efficiency of 99.55%. Furthermore, the cell with FA 4 electrolyte consistently maintained a smaller voltage hysteresis across several cycles than its FA 0 counterpart, alongside more stable deposition/dissolution profiles, as evidenced in Figure 4e, f. In the support information **Figure S15** we observe that the curves after partial amplification remain quite stable, with extremely small voltage variations during cycling, and the curves converge. At the same time, we carry out repetitive verification, as shown in Figure S16, the voltage curves of Zn//Cu cells converge under different cycles. As illustrated in Figure 4g, compared with other recent additive literature, the cycle life, overpotential, concertation, areal capacity, and current density of the Zn//Zn symmetric cells with FA additive were significantly superior to others under the same test conditions (Table S1). This demonstrates the development of a novel additive in this work, which is the trace, suitable for high-rate, low-cost, and high performance.

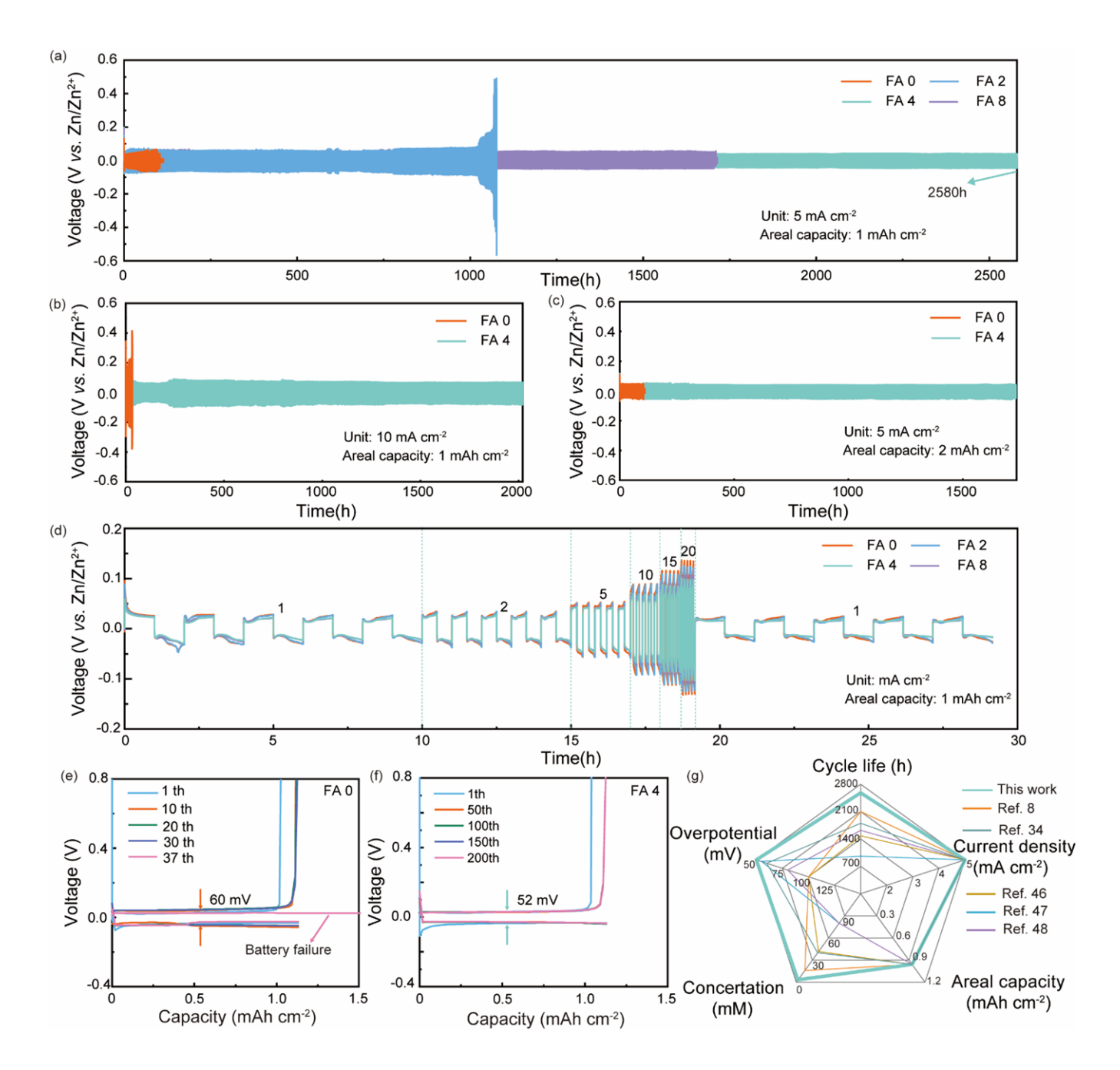


Figure 4. Symmetric cell curves Zn//Zn symmetric cells at a) 5 mA cm⁻²,1 mAh cm⁻², b) 10 mA cm⁻²,1 mAh cm⁻², and c) 5 mA cm⁻²,2 mAh cm⁻². d) The rate curves of symmetric cells in various electrolytes. e) Voltage profiles of Zn//Cu cells in FA 0 electrolyte. f) Voltage profiles of Zn//Cu cells in FA 4 electrolyte. g) Radar chart comparing FA additives to previously reported articles.

Given the exceptional performance of FA additives in stabilizing Zn anodes, it is significant to assess their practical applications. To demonstrate this, we assembled a full battery using V_2O_5 as the cathode and Zn as the anode, with the FA 0 and FA 4 electrolytes. The cyclic voltammetry (CV) curves for cells are displayed in **Figure 5a**. Despite both cells exhibiting analogous redox peaks, the full cell with the FA 4 electrolyte manifests a reduced polarization voltage alongside an elevated current density, signifying

that the incorporation of FA markedly bolsters reaction kinetics while mitigating electrochemical polarization. [46][54] Furthermore, as depicted in **Figure 5b**, electrochemical impedance spectroscopy (EIS) resistance mapping reveals a reduced diameter in the low-frequency region for FA 4 compared to FA 0 electrolyte, coupled with a steeper slope in the high-frequency domain. This suggests a diminished charge-transfer resistance within the full cell utilizing the FA 4 electrolyte, potentially indicative of enhanced Zn²⁺ transfer facilitated by FA adsorption. Figure 5c exhibits the rate performance of the specific capacities of Zn//V₂O₅ cells at current densities of 0.1, 0.5, 1, 2, and 5 A g⁻¹. The results indicate that the electrolyte with the FA 4 electrolyte has a higher specific capacity than the FA 0 electrolyte, demonstrating excellent cell reversibility in the presence of FA. Noteworthy is the observation that while the augmentation in specific capacity at lower rates remains modest, the specificity capacity surges significantly at higher rates upon the inclusion of the FA additives. This dovetails with the rate performance findings observed in Zn//Zn symmetric cells. At the same current density, the full cell of FA 4 electrolyte exhibited longer charge/discharge plateaus at about 1.1 V and 0.5 V than that in FA 0, which aligns with the CV curves and indicates a higher specific capacity (Figure 5d, e). In the full cell system, after 500 cycles, the Zn anodes with FA 0 electrolyte showed severe chalking and dendrite growth. In sharp contrast, in FA 4, the Zn anodes maintained a flat morphology after 500 cycles (Figure 5f). Upon investigating the long-term cycling stability of Zn//V₂O₅ cells at a rate of 5 A g⁻¹, a comparative analysis reveals that the full battery with the FA 4 electrolyte exhibited a higher specific capacity and more excellent cycling stability at approximately the same initial specific capacity compared to the full cell with the FA 0 electrolyte (Figure 5g). All cells display a discernible increase in discharge-specific capacity throughout the initial cycling phases, potentially attributable to the electrolyte's penetration into the V₂O₅ particle interiors, fostering enhanced ion insertion and elevating capacity.^[55,56] This phenomenon has been observed in other Zn//V₂O₅ battery literature.^[46,57–59] Notably, at a high current density of 5 A g⁻¹, the full cell with FA 4 electrolyte exhibits a higher specific capacity enhancement than at 1 A g⁻¹(Figure S14). It maintains excellent cycling stability after 2000 cycles, consistent with the full cell rate performance results. Since electrolyte modification is more of a surface reaction of the cathode material, and most of the stabilization cycles are done under thin electrode conditions with low cathode mass loading, usually in the range of 1~2 mg cm⁻², in order to verify the potential of the additives to be applied in practical production, we conducted a high mass loading (about 5 mg cm⁻²) performance test (**Figure S17**). [60,61] These results demonstrate that FA additives can significantly improve performance at

high rates, paving the way for developing high-rate AZIBs for practical applications.

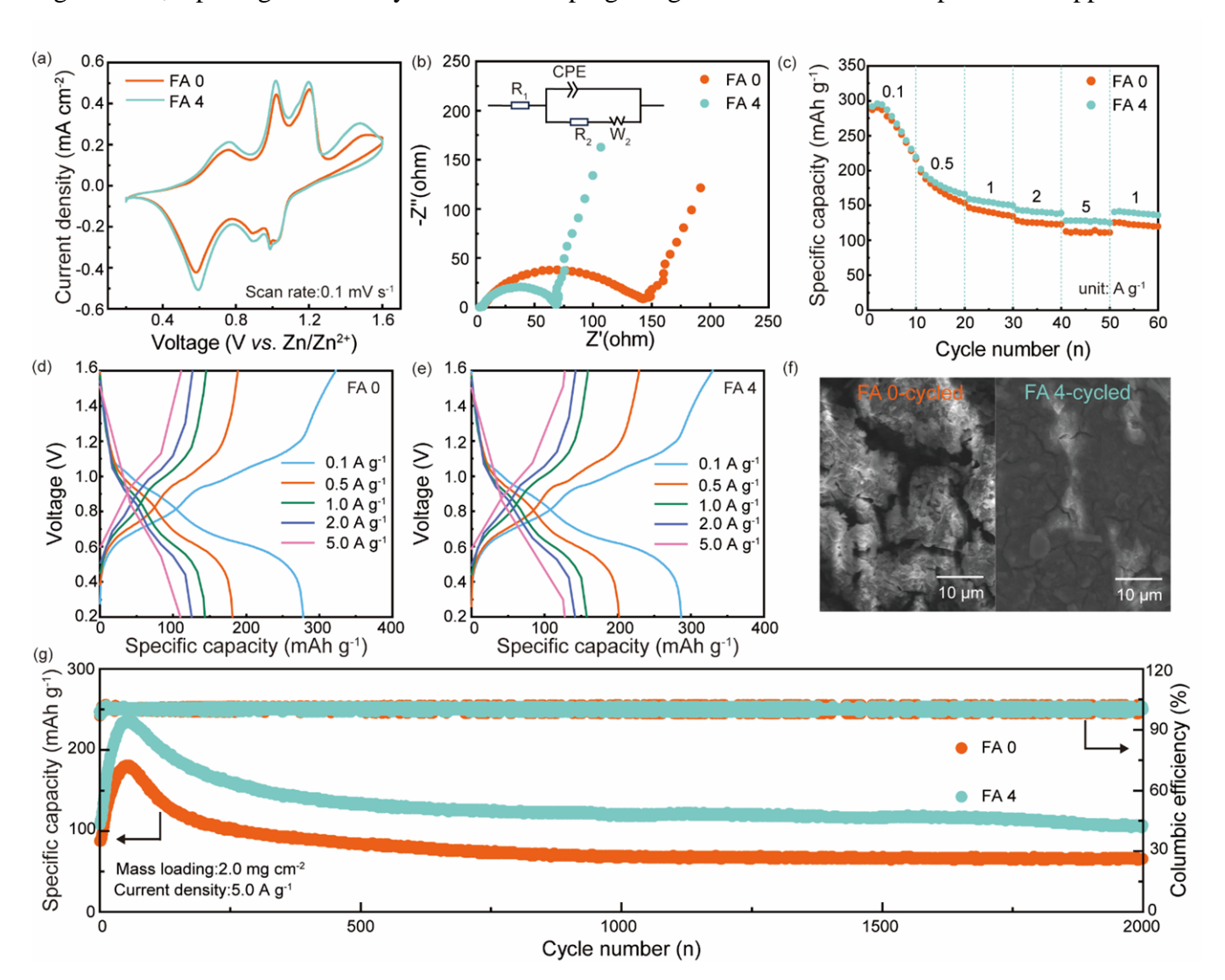


Figure 5. a) CV curves of Zn// V_2O_5 cells with the FA 0 electrolyte and the FA 4 electrolyte. b) EIS curves of the FA 0 electrolyte vs. the FA 4 electrolyte before cycling. c) Multiplication curves of the Zn// V_2O_5 cells. d, e) Charge/discharge curves of the FA 0 electrolyte vs. the FA 4 electrolyte corresponding to multiplicity curves. f) SEM images of Zn anodes with the FA 0 electrolyte and the FA 4 electrolyte after 500 cycles at 5 A g^{-1} ; g) Long cycling performance of Zn// V_2O_5 full cell with the FA 0 electrolyte and the FA 4 electrolyte at 5 A g^{-1} .

3. Conclusion

In summary, this work introduces a novel trace polar additive FA (4mmol) that modulates the EDL structure while adsorbing the Zn anodes surface by chemisorption and forming an *in-situ* SEI layer. Combined with experimental characterization and DFT theoretical simulation calculations, the FA not only forms a water-poor IHP layer *via* preferential adsorption on the surface of the Zn anodes but also interacts with the Zn anodes to form an *in-situ* SEI protective layer, which can inhibit corrosion and

dendrite growth at the interface, as well as inducing the deposition of Zn (002). Utilizing the multiple functions of FA additives, with just tiny quantities of FA, Zn anodes impart an ultra-long lifetime of 2580 hours for Zn//Zn symmetric cells at 5 mA cm⁻²,1 mAh cm⁻² and maintain a lifespan of over 2020 hours even at a high-rate of 10 mA cm⁻², 1 mAh cm⁻². This is a tenfold improvement in the lifespan of the Zn//Cu half-cell over FA 0, along with a high average Coulombic efficiency (CE) of 99.55%. Additionally, the Zn//V₂O₅ full cell with FA 4 electrolyte retains a high capacity of 106.95 mAh g⁻¹ after 2000 cycles at 5 A g⁻¹. This work contributes a novel perspective on selecting multifunctional electrolyte additives that are trace, suitable for high-rate, low-cost, and environmentally friendly *via* considering the relationship between the weak coupling effect, EDL, and *in-situ* SEI layer to regulate the electrochemical performance of the Zn anodes. It provides a novel additive for the design of electrolytes for high-rate AZIBs.

4. Experimental Section

Materials Preparation: This work designed additive concentration gradient experiments. A 2 mol ZnSO₄ electrolyte (FA 0) was prepared by dissolving 6.4588 g of ZnSO₄ in deionized 20 mL (DI) water. Stoichiometric amounts of FA (2 mmol, 4 mmol, and 8 mmol) were dissolved in 2 mol ZnSO₄ electrolyte to prepare electrolytes with preparative FA additives (FA 2, FA 4, and FA 8, respectively). Zn (Ti and Cu) foils (100 μm thick) were firstly cut into 12 mm diameter circular foils, which were ultrasonically cleaned with anhydrous ethanol for 10 minutes and then dried in an oven at 60 °C for 6 hours to remove surface contaminants from the foils. Commercially available vanadium pentoxide (V₂O₅ Macklin 99.99% metal based) was firstly mixed with carbon black (C Aladdin 99.5%), polyvinylidene difluoride (PVDF) in the ratio of 7:2:1 by weight and 1-methyl-2-pyrrolidinone (NMP Aladdin AR>99%) as solvent. The milled and configured slurry was uniformly coated on hydrophilic carbon cloth and dried at 60°C for 12 h before use, and then the carbon cloth was cut into 10 mm diameter discs to serve as cathodes. The loading of the V₂O₅ cathode was controlled to be about 2.0 mg cm⁻². The prepared cell materials are grouped in air into symmetric cells (Zn//Zn), asymmetric cells (Zn//Ti), and full cells (Zn//V₂O₅) with the model CR2032. The electrolyte is 100 μL of 2 M ZnSO₄ solution or 2 M ZnSO₄ + FA solution.

Materials characterization: The XRD patterns were obtained by Rigaku SmartLab 3KW X-ray

diffractometer (Japan) and Cu K α radiation in the 20 range of 5° to 90° at a scan rate. The 1H NMR

(Bruker 400MHz) was performed on the different electrolytes by taking an appropriate sample (about 10

mg) in a 1500 μL centrifuge tube and adding 500 μL D2O. After wholly dissolved, the solution was

transferred and measured into the NMR tube through a pipette gun. The FTIR results were acquired via the Thermo Scientific Nicolet iS20 (American). Before the test, the air background is scanned first, and then a total of 5 μ L of electrolyte is droplet to the crystal surface of the ATR accessory. The infrared spectrum is collected, and the total number of scans is 32 with a resolution of 4 cm⁻¹ and a test range of wave numbers between 400 and 4000 cm⁻¹. Furthermore, the Raman spectra were measured by the HORIBA Scientific LabRAM HR Evolution (Japan, $\lambda = 532$ nm). XPS measurements of the Zn foil surface were conducted under a vacuum with a monochromatic Al K α radiation (Thermo Fischer ESCALAB Xi+, American, 16 mA, 12.5 kV). A Bruker Dimension Icon conducted the AFM measurement of zinc foil under different conditions with a catalyst device. The morphology of zinc foil before and after electrochemical cycling in different electrolytes was obtained by scanning electron microscope (SEM, JSM-6390 LV). The contact angles between electrolytes and Zn electrodes were measured using Dataphysics OCA 20 (German) with 5 μ L of electrolyte for each test. The *in-situ* optical microscope was conducted on RIEVBCAU MS4.

Electrochemical measurements: The BTS 3000 Neware Battery Testing System obtained the electrochemical data of batteries. Long cycling performances of the Zn//Zn symmetric cells with different electrolytes were performed under 10 mA cm⁻² 1 mAh cm⁻², 5 mA cm⁻² 1 mAh cm⁻², and 5 mA cm⁻² 2 mAh cm⁻². respectively. The CS2350M electrochemical workstation tests all electrochemical measurement dates. Electrochemical impedance spectroscopy (EIS) of all samples was measured within a frequent range of 0.01 Hz to 100000 Hz. The Chronoamperometry (CA) curves of Zn//Zn symmetrical cells were tested with an overpotential of -150 mV within 400 s. The Tafel plots of electrolyte were measured with a three-electrode system, with Zn foil as the working electrode, Pt foil as the counter electrode, and Ag/AgCl as the reference electrode. The test range was -1.2 to -0.5 V with a sweep rate of 1 mV s⁻¹. The Cyclic Voltammetry (CV) curves of Zn//Ti cells were measured with a scan range of -0.2-0.8 V and a scan rate of 1 mV s⁻¹. The Zn//V₂O₅ cells have a cyclic voltammetry (CV) curve voltage of 0.2-1.6 V and a scanning rate of 0.5 mV s⁻¹. In the AC voltammetry tests, the frequency is 6 Hz and the amplitude (A) is 25 mV, with a potential range extended from 0.9 to 0.3 V (vs. Zn²⁺/Zn).

DFT Calculations: The first-principles calculations are carried out within the framework of density-functional theory using the projector-enhanced plane-wave method. They are implemented in the Vienna Atomic Bomb Simulation Package.^[62] The generalized gradient approximation of the Perdew, Burke, and Ernzerhof (PBE) functional is applied to the exchange-correlation potential.^[63] Long-range van der Waals

interactions were described by the DFT-D3 method. [64] The first-principles calculations are carried out within the framework of density-functional theory using the projector-enhanced plane-wave method. They are implemented in the Vienna Atomic Bomb Simulation Package. The generalized gradient approximation of the Perdew, Burke, and Ernzerhof (PBE) functional is applied to the exchange-correlation potential. Long-range van der Waals interactions were described by the DFT-D3 method. The Zn (002) plane is constructed of $p(6 \times 6)$ cells with four atomic layers consisting of 144 Zn atoms; a plane wave basis with a kinetic energy cutoff of 500 eV and a Monk horst-Pack scheme with a k-point lattice spacing of $2\pi \times 0.04$ Å⁻¹ were used to ensure convergence of the total energy. [65] The ion and electron optimization convergence conditions were 0.03 eV/Å and 1×10^{-5} eV, respectively. The adsorption energy (E_{ad}) of H₂O and fumaric acid on the Zn (002) plane can be calculated by eq Error! Reference source not found.

$$E_{ad} = E(A+B) - [E(A) + E(B)]$$
 (1)

Where $E_{(A+B)}$ is the energy of the absorption of H₂O or fumaric acid on the Zn (002) plane, $E_{(A)}$ is the energy of the power on the Zn (002) plane, $E_{(B)}$ is the energy of the absorption of H₂O or fumaric acid.

Supporting Information

Supporting Information is available from the Wiley Online Library or from the author.

Acknowledgments

This work was funded by the Startup Fund at Hubei University of Technology and a High-level talent grant from Hubei province.

Conflict of Interest

The authors declare no conflict of interest.

Data Availability Statement

The data that support the findings of this study are available from the corresponding author upon reasonable request.

Reference

- [1] H. Huang, D. Xie, J. Zhao, P. Rao, W. M. Choi, K. Davey, J. Mao, Adv. Energy Mater. 2022, 12, DOI 10.1002/aenm.202202419.
- [2] Y. Wang, T. Wang, Y. Mao, Z. Li, H. Yu, M. Su, K. Ye, D. Cao, K. Zhu, Adv. Energy Mater. 2024,

- 2400353, 1.
- [3] Y. Chen, F. Gong, W. Deng, H. Zhang, X. Wang, Energy Storage Mater. 2023, 58, 20.
- [4] X. Wang, X. Li, H. Fan, L. Ma, Nano-Micro Lett. 2022, 14, 1.
- [5] W. Zhang, Y. Dai, R. Chen, Z. Xu, J. Li, W. Zong, H. Li, Z. Li, Z. Zhang, J. Zhu, F. Guo, X. Gao, Z. Du, J. Chen, T. Wang, G. He, I. P. Parkin, *Angew. Chemie Int. Ed.* 2023, 62, DOI 10.1002/anie.202212695.
- [6] Y. Ding, L. Yin, T. Du, Y. Wang, Z. He, J. A. Yuwono, G. Li, J. Liu, S. Zhang, T. Yang, Z. Guo, Adv. Funct. Mater. 2024, 2314388, 1.
- [7] Z. Hu, F. Zhang, Y. Zhao, H. Wang, Y. Huang, F. Wu, R. Chen, L. Li, *Adv. Mater.* **2022**, 2203104, 1.
- [8] N. Hu, W. Lv, W. Chen, H. Tang, X. Zhang, H. Qin, D. Huang, J. Zhu, Z. Chen, J. Xu, H. He, *Adv. Funct. Mater.* **2024**, *34*, 1.
- [9] W. Li, D. Xu, P. Ruan, Y. Wan, X. Meng, Q. He, K. Liu, Y. Wang, S. Chai, Y. Song, Y. Xie, Z. Chang, A. Pan, Adv. Funct. Mater. 2024, 2404146, 1.
- [10] J. Yang, R. Zhao, Z. Hu, Y. Wang, K. Zhang, Y. Wang, X. Han, A. Zhang, C. Wu, Y. Bai, *Energy Storage Mater.* **2024**, *70*, 103449.
- [11] X. Yang, Q. Zhou, S. Wei, X. Guo, P. J. Chimtali, W. Xu, S. Chen, Y. Cao, P. Zhang, K. Zhu, H. Shou, Y. Wang, X. Wu, C. Wang, L. Song, *Small Methods* **2023**, *2301115*, 1.
- [12] Q. Zhao, W. Liu, X. Ni, H. Yu, C. Zhang, B. Wang, L. Jiang, H. He, Y. Chen, L. Chen, Adv. Funct.
 Mater. 2024, 2404219, 1.
- [13] X. Zhao, X. Zhang, N. Dong, M. Yan, F. Zhang, K. Mochizuki, H. Pan, Small 2022, 18, 1.
- [14] D. Xu, X. Ren, H. Li, Y. Zhou, S. Chai, Y. Chen, H. Li, L. Bai, Z. Chang, A. Pan, H. Zhou, *Angew. Chemie Int. Ed.* **2024**, *63*, DOI 10.1002/anie.202402833.
- [15] M. Mwemezi, S. J. R. Prabakar, S. C. Han, W. B. Park, J. Y. Seo, K. S. Sohn, M. Pyo, *Small* 2022, 18, 1.
- [16] J. Yin, H. Liu, P. Li, X. Feng, M. Wang, C. Huang, M. Li, Y. Su, B. Xiao, Y. Cheng, X. Xu, *Energy Storage Mater.* **2023**, *59*, 102800.
- [17] J. Zheng, Z. Cao, F. Ming, H. Liang, Z. Qi, W. Liu, C. Xia, C. Chen, L. Cavallo, Z. Wang, H. N. Alshareef, ACS Energy Lett. 2022, 7, 197.
- [18] W. Dong, C. Liu, X. Ji, H. Yao, J. Li, H. Du, S. Cheng, Small Methods 2024, 8, 1.

- [19] M. Yang, J. Zhu, S. Bi, R. Wang, H. Wang, F. Yue, Z. Niu, Angew. Chemie 2024, 136, DOI 10.1002/ange.202400337.
- [20] Y. Ai, C. Yang, Z. Yin, T. Wang, T. Gai, J. Feng, K. Li, W. Zhang, Y. Li, F. Wang, D. Chao, Y. Wang, D. Zhao, W. Li, J. Am. Chem. Soc. 2024, 146, 15496.
- [21] X. Xu, M. Song, M. Li, Y. Xu, L. Sun, L. Shi, Y. Su, C. Lai, C. Wang, *Chem. Eng. J.* **2023**, *454*, 140364.
- [22] X. Xu, X. Feng, M. Li, J. Yin, F. Li, J. Chen, W. Shi, Y. Cheng, J. Wang, *Chem. Eng. J.* 2023, 478, 147313.
- [23] C. Li, X. Zhang, G. Qu, S. Zhao, H. Qin, D. Li, N. Li, C. Wang, X. Xu, *Adv. Energy Mater.* **2024**, 2400872, 1.
- [24] J. Liu, C. Li, Q. Lv, D. Chen, J. Zhao, X. Xia, Z. Wu, J. Lai, L. Wang, *Adv. Energy Mater.* **2024**, 2401118, 1.
- [25] K. Wang, T. Qiu, L. Lin, H. Zhan, X. X. Liu, X. Sun, Energy Storage Mater. 2024, 70, 103516.
- [26] Q. Cao, Y. Gao, J. Pu, X. Zhao, Y. Wang, J. Chen, C. Guan, Nat. Commun. 2023, 14, 1.
- [27] L. Liu, X.-Y. Wang, Z. Hu, X. Wang, Q. Zheng, C. Han, J. Xu, X. Xu, H.-K. Liu, S.-X. Dou, W. Li, Angew. Chemie 2024, 202405209, DOI 10.1002/ange.202405209.
- [28] J. Chen, N. Liu, W. Dong, Y. Xu, Y. Cao, S. Zhang, J. Hou, H. Bi, T. Lin, F. Q. Huang, *Adv. Funct. Mater.* **2024**, *2313925*, 1.
- [29] S. Zhang, Q. Gou, W. Chen, H. Luo, R. Yuan, K. Wang, K. Hu, Z. Wang, C. Wang, R. Liu, Z. Zhang, Y. Lei, Y. Zheng, L. Wang, F. Wan, B. Li, M. Li, Adv. Sci. 2024, 2404968, 1.
- [30] H. Wang, H. Wang, W. Zhang, L. Yan, S. Yao, J. Mater. Chem. A 2024, 12, 6376.
- [31] M. R. Shaik, S. M. Olidan, J. Kim, K. Y. Cho, S. Yoon, J. Mater. Chem. A 2023, 11, 6403.
- [32] L. Jiang, D. Li, X. Xie, D. Ji, L. Li, L. Li, Z. He, B. Lu, S. Liang, J. Zhou, *Energy Storage Mater*.2023, 62, DOI 10.1016/j.ensm.2023.102932.
- [33] L. Deng, X. Xie, W. Song, A. Pan, G. Cao, S. Liang, G. Fang, Chem. Eng. J. 2024, 488, 151104.
- [34] Z. Shen, J. Mao, G. Yu, W. Zhang, S. Mao, W. Zhong, H. Cheng, J. Guo, J. Zhang, Y. Lu, Angew. Chemie 2023, 135, DOI 10.1002/ange.202218452.
- [35] M. Han, J. Zhang, C. Yu, J. Yu, Y. Wang, Z. Jiang, M. Yao, G. Xie, Z. Yu, J. Qu, *Angew. Chemie* 2024, 136, DOI 10.1002/ange.202403695.
- [36] C. Yan, H. R. Li, X. Chen, X. Q. Zhang, X. B. Cheng, R. Xu, J. Q. Huang, Q. Zhang, J. Am. Chem.

- Soc. 2019, 141, 9422.
- [37] S. Mao, J. Mao, Z. Shen, Q. Wu, S. Zhang, J. Zhang, Y. Lu, *Nano Lett.* **2023**, 23, 7014.
- [38] C. Li, G. Qu, X. Zhang, C. Wang, X. Xu, Energy Environ. Mater. 2024, 7, 1.
- [39] T. Wu, C. Hu, Q. Zhang, Z. Yang, G. Jin, Y. Li, Y. Tang, H. Li, H. Wang, *Adv. Funct. Mater.* **2024**, *34*, 1.
- [40] Y. Dong, N. Zhang, Z. Wang, J. Li, Y. Ni, H. Hu, F. Cheng, J. Energy Chem. 2023, 83, 324.
- [41] Y. Yu, P. Zhang, W. Wang, J. Liu, Small Methods 2023, 7, 1.
- [42] Y. Yang, Y. Li, Q. Zhu, B. Xu, Adv. Funct. Mater. 2024, 2316371, 1.
- [43] A. Chen, C. Zhao, J. Gao, Z. Guo, X. Lu, J. Zhang, Z. Liu, M. Wang, N. Liu, L. Fan, Y. Zhang, N. Zhang, *Energy Environ. Sci.* **2022**, *16*, 275.
- [44] R. Chen, W. Zhang, Q. Huang, C. Guan, W. Zong, Y. Dai, Z. Du, Z. Zhang, J. Li, F. Guo, X. Gao,
 H. Dong, J. Zhu, X. Wang, G. He, *Nano-Micro Lett.* 2023, 15, 1.
- [45] K. Lu, G. Yuan, H. Tan, P. Wang, J. Ye, L. Huang, J. Power Sources 2024, 613, 234830.
- [46] H. Dong, S. Yan, T. Li, K. Ming, Y. Zheng, Z. Liu, G. Li, J. Liu, H. Li, Q. Wang, X. Hua, Y. Wang, J. Power Sources 2023, 585, 233593.
- [47] K. Ouyang, F. Li, D. Ma, Y. Wang, S. Shen, M. Yang, J. Qiu, W. Wen, N. Zhao, H. Mi, P. Zhang, *ACS Energy Lett.* **2023**, *8*, 5229.
- [48] T. Shen, M. Fang, T. Lv, H. Wu, O. Sheng, T. Yang, C. Dong, H. Ji, E. Zhang, X. Zhang, C. Zhang,
 R. Zheng, J. Zhang, X. Zhang, Adv. Funct. Mater. 2024, 2408578, 1.
- [49] P. Wang, H. Zhou, Y. Zhong, X. Sui, G. Sun, Z. Wang, Adv. Energy Mater. 2024, 2401540, 1.
- [50] C. Yi, L. Jiao, J. Wang, Y. Ma, H. Bai, Q. Liu, S. Wang, W. Xin, Y. Lei, T. Zhang, L. Yang, D. Shu, S. Yang, K. Li, C. Li, H. Li, W. Zhang, B. Cheng, Adv. Funct. Mater. 2024, 2404579, 1.
- [51] X. Xiao, X. Ye, Z. Wu, X. Wu, J. Yu, L. Gu, S. Liu, Adv. Mater. 2024, 2408706, 1.
- [52] X. Shi, J. Xie, J. Wang, S. Xie, Z. Yang, X. Lu, Nat. Commun. 2024, 15, DOI 10.1038/s41467-023-44615-y.
- [53] H. Yu, D. Chen, Q. Li, C. Yan, Z. Jiang, L. Zhou, W. Wei, J. Ma, X. Ji, Y. Chen, L. Chen, *Adv. Energy Mater.* **2023**, *13*, 1.
- [54] X. Sun, X. Lv, M. Zhang, K. Shi, Z. Li, X. Pan, T. Lian, R. Chen, F. Wu, L. Li, ACS Nano 2024, 18, 8452.
- [55] H. Kim, J. C. Kim, M. Bianchini, D. H. Seo, J. Rodriguez-Garcia, G. Ceder, Adv. Energy Mater.

- **2018**, 8, 1.
- [56] D. Kundu, S. Hosseini Vajargah, L. Wan, B. Adams, D. Prendergast, L. F. Nazar, *Energy Environ. Sci.* 2018, 11, 881.
- [57] G. Duan, Y. Wang, L. Sun, Z. Bao, B. Luo, S. Zheng, Z. Ye, J. Huang, Y. Lu, ACS Nano 2023, 17, 22722.
- [58] J. Cui, X. Liu, Y. Xie, K. Wu, Y. Wang, Y. Liu, J. Zhang, J. Yi, Y. Xia, Mater. Today Energy 2020, 18, 100563.
- [59] J. Weng, W. Zhu, K. Yu, J. Luo, M. Chen, L. Li, Y. Zhuang, K. Xia, Z. Lu, Y. Hu, C. Yang, M. Wu, Z. Zou, Adv. Funct. Mater. 2024, 34, 1.
- [60] X. Gao, C. Shen, H. Dong, Y. Dai, P. Jiang, I. P. Parkin, H. Zhang, C. J. Carmalt, G. He, *Energy Environ. Sci.* 2024, 17, 2287.
- [61] Z. Xu, Z. Sun, J. Shan, S. Jin, J. Cui, Z. Deng, M. H. Seo, X. Wang, *Adv. Funct. Mater.* 2024, 34,1.
- [62] D. Joubert, Phys. Rev. B Condens. Matter Mater. Phys. 1999, 59, 1758.
- [63] K. Li, L. Luo, Y. Zhang, W. Li, Y. Hou, ACS Appl. Mater. Interfaces 2018, 10, 41525.
- [64] S. Grimme, J. Antony, S. Ehrlich, H. Krieg, J. Chem. Phys. 2010, 132, DOI 10.1063/1.3382344.
- [65] J. D. Pack, H. J. Monkhorst, *Phys. Rev. B* **1977**, *16*, 1748.